Analytical and Bioanalytical Chemistry
https://doi.org/10.1007/s00216-018-0869-1

RESEARCH PAPER

Characterization of the NISTmAb Reference Material using small-angle scattering and molecular simulation

Part II: Concentrated protein solutions

Maria Monica Castellanos[1,2,3] · Kevin Mattison[4] · Susan Krueger[1] · Joseph E. Curtis[1]

Received: 26 September 2017 / Revised: 11 December 2017 / Accepted: 10 January 2018

Abstract
Protein-protein interactions in monoclonal antibody solutions are important for the stability of a therapeutic drug and directly influence viscosity in concentrated protein solutions. This study describes the use of small-angle scattering to estimate protein-protein interactions at high concentrations of the IgG1 NISTmAb reference material and validate colloidal models for interacting molecules. In particular, we studied the colloidal stability of the NISTmAb at high protein concentrations and analyzed protein-protein interactions upon adding sodium chloride and its effect on viscosity. Isotropic colloidal models for interacting molecules were combined with an ensemble of atomistic structures from molecular simulation to account for the flexibility of the NISTmAb in solution. In histidine formulation buffer, net repulsive electrostatic interactions are important for the colloidal stability of the NISTmAb at high concentrations. Addition of sodium chloride increased the viscosity of the NISTmAb and decreased the colloidal stability due to charge screening of the repulsive interactions. The interactions at high concentrations (up to ~ 250 mg/mL) were consistent with those from light scattering at low concentrations (below ~ 20 mg/mL). However, in the presence of sodium chloride, the screening of charges was less pronounced with increasing protein concentration and the interactions approached those of the repulsive hard-sphere models. Additionally, we studied the NISTmAb under frozen conditions using in situ neutron scattering to analyze the crowded state as proteins are excluded from the water-rich phase. In the frozen samples, where protein concentration can reach hundreds of mg/mL in the protein-rich phase, sodium chloride did not affect the molecular spacing and crowding of the NISTmAb.

Keywords Small-angle scattering · NISTmAb reference material · Protein-protein interactions · Concentrated protein solutions · Frozen protein solutions

Introduction

In the development of therapeutic products, low propensity for aggregation and low viscosities are desirable for manufacturing and subcutaneous delivery of the protein drugs [27, 28, 34]. Because therapeutic proteins are typically formulated and stored as concentrated solutions (c > 100 mg/mL) understanding protein-protein interactions (PPI) at high concentrations can aid in the design of biotherapeutics.

In order to assess any potential issues with aggregation or viscosities, biophysical characterization techniques are often used to investigate protein-protein interactions and structural integrity in the native state in different formulation buffers and upon exposing the protein to a stressed environment. Although there are numerous techniques available to characterize therapeutic proteins, there is not a single technique that

✉ Joseph E. Curtis
joseph.curtis@nist.gov

[1] NIST Center for Neutron Research, National Institute of Standards and Technology, 100 Bureau Drive, Mail Stop 6102, Gaithersburg, MD 20899, USA

[2] Institute for Bioscience and Biotechnology Research, University of Maryland, 9600 Gudelsky Drive, Rockville, MD 20850, USA

[3] Present address: Drug Product Development US, GSK Vaccines, 14200 Shady Grove Rd, Rockville, MD 20850, USA

[4] Malvern Instruments, 117 Flanders Road, Westborough, MA 01581, USA

Published online: 08 February 2018

provides a complete biophysical profile of the molecule and orthogonal techniques are generally required [6].

As described in the first part of these papers on small-angle scattering of the NISTmAb Primary Sample 8670 (NISTmAb) [8], small-angle scattering is a suitable technique to study structure and correlations in a system, because of its sensitivity to the spatial relation of atoms in the sample. Besides containing information on the distribution of atoms in the molecule, small-angle scattering can provide insights on the arrangement of molecules as protein concentration increases. Among other factors, the molecular structure of a complex fluid is dependent upon PPI, because molecules will arrange in solution to minimize the free energy of the system. Although small-angle scattering is a low resolution technique, changes in intermolecular correlations due to protein-protein interactions result in different scattering profiles, which can be used to validate theoretical models of interacting molecules at high concentrations.

Once information about the dilute condition of the system has been obtained, small-angle scattering can be used to study correlations in concentrated solutions using the effective structure factor $S'(Q)$ [19]:

$$S'(Q) = \frac{I(Q)}{\phi V_p (\Delta\rho)^2 P(Q)}, \quad (1)$$

where Q is momentum transfer ($Q = 4\pi \sin(\theta)/\lambda$ where 2θ is the scattering angle and incident wavelength λ), $I(Q)$ is the scattered intensity of molecules with volume Vp, ϕ is the volume fraction and $P(Q)$ is the form factor. In dilute solutions, $S'(Q) = 1$ and the Q dependence of the scattering comes from $P(Q)$. However, as protein concentration increases, $S'(Q) \neq 1$ indicating that the molecular arrangement is affected by neighboring molecules. Details on the correlation between $S'(Q)$ and the pairwise interaction energy can be found in the literature [12, 19, 20]. Briefly, if $S'(Q) < 1$, the net interaction of the system is repulsive, whereas if $S'(Q) > 1$, the net interaction of the system is attractive. If $S'(Q) = 1$, the molecules are not affected by the presence of other molecules (no interaction). This metric is comparable to the commonly used second virial coefficient B_{22} measured with static light scattering. However, while B_{22} is valid only at low concentrations, $S'(Q)$ is applicable at high concentrations.

Intermolecular interactions of monoclonal antibodies have been analyzed using small-angle scattering (SAS). For example, the origins of a non-Newtonian rheology in a monoclonal antibody solution were identified using small-angle neutron scattering (SANS) from analyzing PPI at high concentrations [9]. Anisotropic interactions and formation of reversible clusters in concentrated antibody solutions was observed using SANS and correlated with the viscosity of the solutions [17, 36, 37]. Note that the identification of clusters from SAS experiments derives from analysis using models to interpret the data, thus there they are not identified by direct observation. Other studies have used small-angle X-ray scattering (SAXS) to determine the net interactions in antibody solutions under different formulations [21, 25].

Although most small-angle scattering studies have been performed at low concentration, perhaps because small-angle scattering in biotechnology has historically focused on structural studies, small-angle scattering in concentrated solutions can yield key information on PPI that can guide the development of biotherapeutics, such as choosing formulations that result in satisfactory biophysical profiles. Moreover, the strength and range of PPI can be analyzed by modeling the Q dependence on the $S'(Q)$ profile. Theoretical and computational models are available to quantitatively analyze protein interactions. Although computational models can be useful for better designing biotherapeutics and understanding their macroscopic behavior, all models should be validated against experimental data. Similar to the dilute solution case, small-angle scattering experiments can be used to check if theoretical and computational models are properly representing the experimental system of interacting proteins.

SANS has the unique advantage that it can be combined with a wide range of instrumentation, allowing the in situ monitoring of the protein structure in different phases under a wide range of conditions, such as low temperatures, high pressure, and shear flow, among others that are under development. For example, SANS can be used to monitor structural changes below the freezing point [14, 15]. Therefore, the researcher can qualitatively learn about the conformational stability during freezing and thawing of a protein sample, and investigate reversibility, aggregate formation, and effects of excipients. Lyophilized protein powders can also be studied with small-angle scattering [11, 14].

In this study, we describe small-angle scattering data on the NISTmAb at high protein concentrations. All samples described herein were studied in 25 mM histidine formulation buffer with either 0 or 150 mM NaCl (1000 mM = 1 M = 1 mol/L). Analytical characterization of the NISTmAb Reference Material has been published in a collection of three volumes of the book "State-of-the-Art and Emerging Technologies for Therapeutic Monoclonal Antibody Characterization" [30–32]. For this manuscript, we present SANS data at room temperature up to concentrations of ~ 250 mg/mL. Because the solution structure at dilute conditions has been throughly studied [8], we then calculated $S'(Q)$ profiles to evaluate PPI. We show how colloidal models can be used to describe the effect of NaCl on the NISTmAb interactions and analyze $S'(Q)$ profiles while accounting for structural flexibility of the NISTmAb. We compared the experimentally measured charge with the parameters obtained from the models and compared changes in viscosity with differences in PPI. Finally, we studied the amorphous state of frozen NISTmAb samples at −80 °C. Molecular crowding was observed as the molecules

showed an average separation distance much smaller than their radius of gyration, *Rg*, observed in dilute conditions.

Methods

The NISTmAb Primary Sample 8670 was provided by the National Institute of Standards and Technology (NIST) in frozen vials at concentrations of 10 and 100 mg/mL. Vials were thawed overnight at 4 °C. The NISTmAb solutions were buffer-exchanged and concentrated using Amicon Ultra-15 centrifugal filters (Millipore, UFC903024)[1] with a 30 kDa molecular-weight cutoff in a swinging bucket centrifuge (Thermo Scientific, Sorvall ST 40R Centrifuge, 75004525) at 4000 relative centrifugal force. Buffer solution was added to the retentate in six cycles to reach >99.9% of the desired buffer. All samples were prepared in 25 mM histidine buffer with either 0 or 150 mM NaCl (Sigma Aldrich, S9888). A deuterated buffer was used to minimize the contribution of incoherent background on the scattering. We have shown that D_2O does not affect the solution structure of the NISTmAb [8]. The deuterated histidine buffer contained 12.5 mM L-Histidine Monohydrochloride (JT Baker, JT2081-6) and 12.5 mM L-Histidine (JT Baker, JT2080-5) in 99.9% D_2O (Sigma-Aldrich, 151882) and was adjusted to pD = 6.4 (pH = 6.0) with a 1 M sodium deuteroxide solution (Sigma Aldrich, 372072) before filtering with a 0.2 μm filter. Samples were measured within three days of preparation at 25 °C unless otherwise specified.

The NG7 and NGB 30 m SANS instruments at the NIST Center for Neutron Research were used for the SANS measurements. The neutron wavelengths λ were 6 and 8.4 Å, with a wavelength spread δλ/λ of 0.15 Å. A two-dimensional 64 cm × 64 cm position-sensitive detector with 128 × 128 pixels at a resolution of 0.5 cm/pixel was used to detect scattered neutrons. The SANS macro routines developed at the NCNR in the Igor Program were used for data reduction [22]. Raw counts were normalized to a common monitor count and corrected for empty cell counts, ambient room background counts and non-uniform detector response. All data were isotropic and therefore radially averaged to produce a 1D scattered intensity, $I(Q)$, versus Q profiles. Scattering profiles were scaled to account for protein concentration using an arbitrary factor, which was obtained from using Porod's law at Q values >0.3 $Å^{-1}$.

Three sample-to-detector distance configurations were used (1.3, 4.0 and 13.4 m) to cover a Q range of 0.003 $Å^{-1} < Q < 0.45$ $Å^{-1}$ in the liquid solution measurements. For the frozen samples, the Q range was of 0.005 $Å^{-1} < Q < 0.22$ $Å^{-1}$. Scattered intensities were calculated after accounting for buffer scattering and incoherent scattering from hydrogen. Although the background could not be directly subtracted for the frozen samples, because of the low-Q scattering of the buffer [14, 15], the scattering was corrected by approximately subtracting a constant background at all Q values.

For the frozen studies, NISTmAb solutions were placed in 1 mm path length demountable titanium cells with titanium windows. Samples were loaded at 25 °C and the temperature was decreased to 10, 5, 0, −5, −10, −20, −40 and −80 °C, defined as the slow cooling rate. For the fast cooling rate, the temperature was decreased directly from 25 to −80 °C. In all cases, the sample remained at the specified temperature for at least 30 min before collecting data and changing to a different temperature. Scattering measurements were taken at each temperature using two configurations, and measurements at a single configuration were taken during temperature changes.

The colloidal model fitting was performed using the SANS analysis macros developed at the NCNR in the Igor Program [22] and an Igor procedure developed for this study to fit several scattering profiles in a single run. Only the low-Q region of the $S'(Q)$ profile was used for the fitting, that is, $Q \leq 0.04$ $Å^{-1}$. The volume fraction ϕ was calculated from the measured protein concentration c as $\phi = (\overline{v}_p + \overline{v}_w\ \delta)c$, where $\overline{v}_p$ and $\overline{v}_w$ correspond to the partial specific volume of the protein and water respectively, and δ is the mass of hydration water per mass of protein. $\overline{v}_p$ of 0.71 mL/g was determined from the volume from the atomistic structures and the molecular weight, whereas the value of δ was obtained from the literature as 0.59 g/g [7]. $S('0)$ values were obtained by doing an expansion of $S'(Q)$ and calculating the intercept of a linear regression of the experimental data in the Q region below 0.01 $Å^{-1}$ as described in reference [2]. The r^2 values of the fit were 0.97 or higher.

The ensembles of structures used for the $S'(Q)$ analysis were obtained from molecular simulations using SASSIE [5, 16, 26] as described in the NISTmAb study at dilute conditions [8]. The ensemble of all structures refers to the 136,568 structures from torsion-angle Monte Carlo simulation, and the ensemble of best structures represents 861 structures that best matched the experimental scattering data. The experimental $S'(Q)$ was obtained from the experimental $I(Q)$ and $P(Q)$ at dilute conditions using Eq. 1. The same expression was used for the ensemble analysis, by solving for $I(Q)$ with the $P(Q)$ used to evaluate the quality of agreement to the model structures [8] and the experimental $S'(Q)$. This result and the scattering profile of each configuration ($P(Q)$) were used to calculate ensembles of $S'(Q)$ profiles. SASSIE was used to calculate an ensemble of $P(Q)$ in order to predict the ensemble of $S'(Q)$ profiles. The models derived from SASSIE do not include protein-protein interactions.

[1] Certain commercial equipment, instruments, materials, suppliers, or software are identified in this paper to foster understanding. Such identification does not imply recommendation or endorsement by the National Institute of Standards and Technology, nor does it imply that the materials or equipment identified are necessarily the best available for the purpose.

To check for irreversible aggregation, a UV detection based high performance size exclusion chromatography (HP-SEC Thermo Scientific/Dionex U3000) system was used. The system consisted of a HPG 3400 binary pump (Thermo Fisher Scientific, 5040.0046), a thermostatted WPS-3000TRS autosampler (Thermo Fisher Scientific, 5840.0020), a thermostatted column compartment TCC-3000RS (Thermo Fisher Scientific, 5730.0000), and a four channel variable wavelength detector (Thermo Fisher Scientific, 5074.0010). The mobile phase was 10 mM phosphate buffer saline solution with 138 mM NaCl at pH 7.4. Samples were not diluted prior to injection and thus the injected volume was dependent upon the concentration of protein in each sample. A TSKgel G3000SWxl column (Tosoh Bioscience, 08541) was used for separation. Absorbance was measured at 280 nm. The flow rate was 0.45 mL/min. The limits of detection and quantification for this method have been estimated as 0.026 and 0.086% respectively.

The viscosity of the NISTmAb formulation at 25 ± 0.1 °C was determined in duplicates using a Viscosizer Taylor Dispersion Analysis system (Malvern Instruments). The Viscosizer system utilizes a dual pass UV detector to measure the velocity of a sample front as it moves through a 75 m ID hydroxypropyl cellulose coated capillary under constant pressure. The relative viscosity η_{Rel} of the sample was calculated according to Eq. 2, where η_{sp} is the specific viscosity, L is full length of the capillary, l_1 and l_2 are the distances to the 1st and 2nd detection windows, t is the time required for the front to move from window 1 to window 2, and the S and B subscripts represent sample and buffer respectively.

$$\eta_{Rel} = \eta_{sp} + 1 = \left(\frac{2L}{l_1 + l_2}\right)\left(\frac{\Delta t_S - \Delta t_B}{\Delta t_B}\right) + 1 = \frac{\eta_S}{\eta_B} \qquad (2)$$

The capillary was first filled with buffer. The sample was then injected in a continuous fashion, until the buffer was completely displaced from the capillary, facilitating measurement of the leading front t_B. The final step was to displace the sample within the capillary using a buffer push, which facilitated measuring the trailing front t_S. The relative viscosity of the buffer was then determined by repeating the process, but using buffer as the sample and water as the push. Using the known viscosity of water, the absolute viscosities of both the buffer and the sample were calculated from Eq. 2. Run pressures of 1000 and 2000 mbar were used and the resulting shear rates ranged from ~ 100 to 3000 s^{-1}. No evidence of non-Newtonian behavior was found. Caffeine at 1 mg/ml was used as a UV marker for the buffer viscosity measurement.

The effective charge Z_{Eff} of the NISTmAb at 25 ± 0.1 °C was determined using a Zetasizer Nano ZSP system (Malvern Instruments), according to the expression $Z_{Eff} = 6\pi\mu_E\eta R_S/e$, where μ_E is the electrophoretic mobility, η is the sample viscosity, R_S is the Stokes radius, and e is the elemental charge. The Stokes radius, defined as the hydrodynamic radius under ideal solution conditions, e.g. in the limit of zero particle interactions, was measured in the same instrument using dynamic light scattering (DLS). The Zetasizer utilizes the electrophoretic light scattering (ELS) technique to measure μ_E. The sample was subjected to an oscillating electric field of constant voltage, with the electrophoretic velocity of the macromolecules being determined from a phase analysis of the Doppler frequency shifted scattered light. μ_E is proportional to the frequency shift Δf per unit field strength E, according to $\mu_E = \lambda\Delta f/(2E\sin(\theta/2))$, where λ is the incident light wavelength and θ is the observation or scattering angle. The electrophoretic mobility of a 10 mg/ml sample was measured in a disposable folded capillary cell using the diffusion barrier technique with an applied voltage of 150 V and 50 sub-runs per measurement. The average mobility was calculated across 15 automated measurements. The Stokes radius was then calculated using the Stokes-Einstein relation with the self diffusion coefficient D_0 measured in the limit of infinite dilution. D_0 was determined using concentration ladders (~ 1–10 mg/ml), with D_0 being the Y-intercept of the concentration dependent DLS measured diffusion coefficients. The resulting Stokes radii were 53 and 54 Å for the NISTmAb samples with 0 and 150 mM NaCl respectively.

Results

To analyze the effect of high protein concentrations on the formation of irreversible aggregates, size-exclusion chromatograms (SEC) of NISTmAb solutions were obtained. The results are presented in Fig. 1, that correspond to solutions

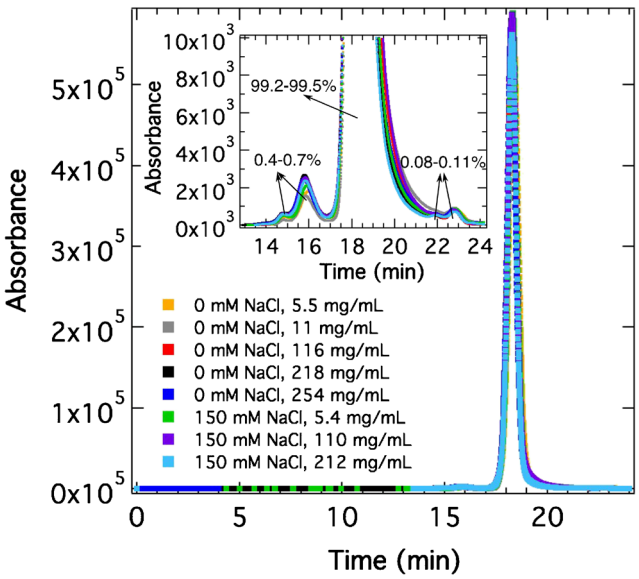

Fig. 1 Size-exclusion chromatography data for solutions of NISTmAb. Inset displays a closer view of the smallest peaks from the SEC chromatogram; note the two orders of magnitude difference in the y-axis

stored at 4 °C for up to two weeks at different protein concentrations and with 0 and 150 mM NaCl. Monomer purities higher than 99.2% and low content of high-molecular-weight (HMW) species (less than 0.7%) were observed in all samples, even at concentrations as high as 254 mg/mL. Therefore, irreversible aggregation did not occur in NISTmAb solutions as a result of increasing protein concentration.

Figure 2 displays the normalized scattering profiles of the NISTmAb in histidine buffer and with 150 mM of added NaCl. As protein concentration increased, proteins interacted with neighboring protein molecules and the increased correlations affected the scattering profiles at low and intermediate Q. In the absence of NaCl, a change in the scattering profile occured at concentrations of ~ 10 mg/mL and above. Because the scattered intensity decreased with increasing protein concentration, the system experienced net repulsive interactions under these conditions. Moreover, the peak in the intensity at the intermediate Q range of 0.02 $Å^{-1} < Q < 0.1$ $Å^{-1}$ corresponds to the nearest neighbor peak and provides information on the average separation distance between molecules. This peak shifted to higher Q (smaller distance) as the system became crowded. On the contrary, adding salt leads to a scattering profile that remained invariant at the lowest concentrations studied; intermolecular interactions were not detected until the concentration increased above ~ 50 mg/mL. Moreover, the nearest neighbor peak was not as pronounced as in the case with 0 mM NaCl, although net repulsive interactions also dominated with 150 mM NaCl.

The net intermolecular interactions were investigated by calculating the effective structure factor $S'(Q)$. Figure 3 presents $S'(Q)$ as a function of protein concentration under the same conditions as in Fig. 2. For all concentrations and conditions, the system experienced net repulsive interactions as $S'(Q) < 1$ at low and intermediate Q. Comparing $S'(Q)$ profiles at similar concentrations, repulsive interactions were much

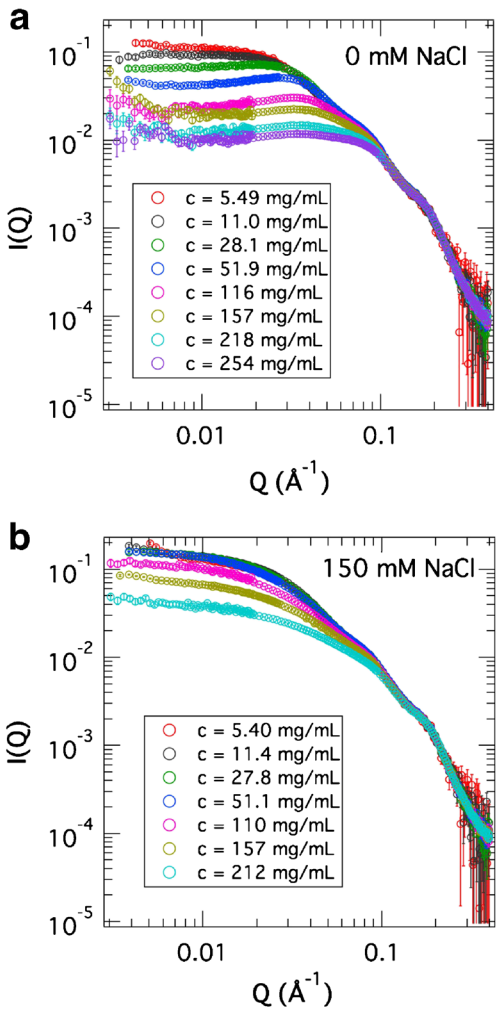

Fig. 2 SANS profiles for concentrated NISTmAb solutions in histidine buffer with **a** 0 mM NaCl, and **b** 150 mM NaCl. For comparison purposes, profiles were relatively scaled according to the concentration of protein. Error bars correspond to ±1 the propagated standard error

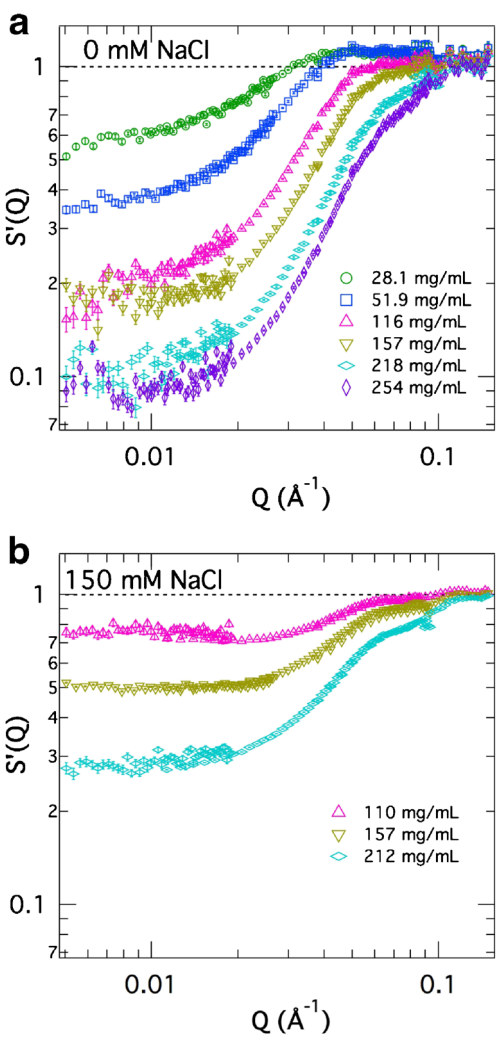

Fig. 3 Effective structure factor for concentrated NISTmAb solutions. **a** 0 mM NaCl **b** Adding 150 mM NaCl. Error bars correspond to ±1 the propagated standard error

weaker in samples with NaCl as the $S'(Q)$ values were higher than in the case with 0 mM NaCl.

Isotropic colloidal models were used to assess the strength and range of interactions by fitting the low-Q region of the scattering profile [10]. Three models were used as follows: the hard sphere model representing only the steric (hard-core) repulsion between molecules; the Hayter and Penfold model [20], which additionally includes an electrostatic repulsion between the molecules; and the two-Yukawa model [13, 24], which includes an attractive interaction besides steric and electrostatic repulsion. The experimental data and the models are represented in Fig. 4a, which compares the $S'(Q)$ profiles for the two conditions studied (0 and 150 mM NaCl) with the profile of a hard sphere model at similar conditions. The Hayter and Penfold model, representing electrostatic repulsion, was used to fit the experimental data with 0 mM NaCl

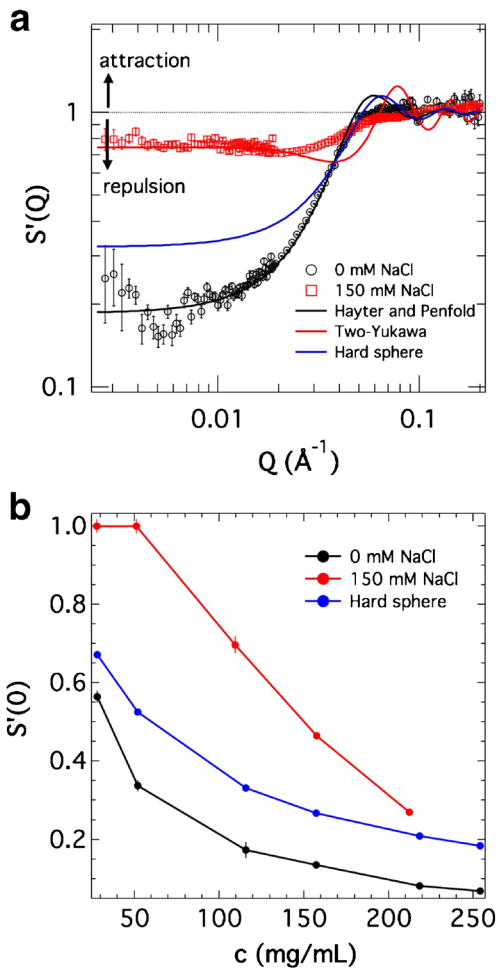

Fig. 4 **a** Effective structure factor at 116 and 110 mg/mL with 0 and 150 mM NaCl respectively. Profiles are compared with the structure factor of a hard sphere with diameter 90 Å and an equivalent concentration of 116 mg/mL. Lines correspond to model fits as described in the legend. Dashed line represents the condition where the net intermolecular interactions are zero. **b** Structure factor at $Q = 0$. Lines in **b** are used to guide the eye. Error bars correspond to ±1 the propagated standard error

in the low-Q region (up to ~ 0.05 Å^{-1}). For the samples with 150 mM NaCl, both repulsive and attractive interactions (Two-Yukawa model) were needed to fit the low-Q region of the experimental data. Although the net interaction of the system is repulsive in both cases, the steric repulsion, resulting from molecules not able to occupy the same volume, contributed to a repulsive interaction that had to be balanced by an attractive interaction in the samples with NaCl. In the case of antibodies, their non-globular shape and flexibility can contribute to correlations at distances smaller than the hard-core diameter, for example when antibodies interdigitate, which can result in an apparent attractive interaction. One should note that the statistical mechanical models exhibit correlation peaks at Q > 0.05 Å^{-1} that are not present in the experimental data as has been noted for another protein samples [10]. The uniformity of the geometric models do not adequately capture the structural heterogeneity of the NISTmAb in solution and therefore one should consider the correlation peaks as artifacts of the models. Figure 4b compares $S'(Q)$ at $Q = 0$, which correlates with the osmotic compressibility of protein solutions as a measure of thermodynamic non-ideality [12, 35]. The values of $S'(0)$ confirmed that both repulsive interactions (electrostatic) and the steric repulsion contribute to the net interactions in the 0 mM NaCl solutions, whereas the samples with NaCl were less repulsive than a system with only steric interactions. Nevertheless, as protein concentration increased to 212 mg/mL, $S'(0)$ of the solutions with 150 mM NaCl approached $S'(0)$ of the most repulsive models, such as the hard sphere. Note that changes in $S'(0)$ with concentration were similar for the NISTmAb without NaCl and the hard sphere model; the difference represents the electrostatic contribution, which remained nearly identical at all concentrations.

Because monoclonal antibodies are flexible molecules and do not have a single configuration (structure) in solution, we evaluated the effect of configurational fluctuations on the $S'(Q)$ profiles and how these fluctuations may affect the model parameters describing the system. We obtained $S'(Q)$ for the same ensembles of flexible structures used in the NISTmAb study at dilute conditions [8] with 0 mM salt. Figure 5 displays the effect of configurational fluctuations on $S'(Q)$ as a result of molecular flexibility in the NISTmAb. Two ensembles of structures were considered: all structures from torsion-angle Monte Carlo simulations (all structures), and structures that best match the experimental data (best structures) [8]. These results showed that all $S'(Q)$ profiles converged to the same value as $Q \rightarrow 0$. Most fluctuations occured in the intermediate Q range of 0.06 Å^{-1} < Q < 0.1 Å^{-1}.

To analyze the effects of configurational fluctuations on the choice of a colloidal model and its resulting parameters, the model of Hayter and Penfold (electrostatic interactions) was used to fit each $S'(Q)$ profile of the ensembles. Table 1 shows the resulting charge and diameter of the molecule obtained

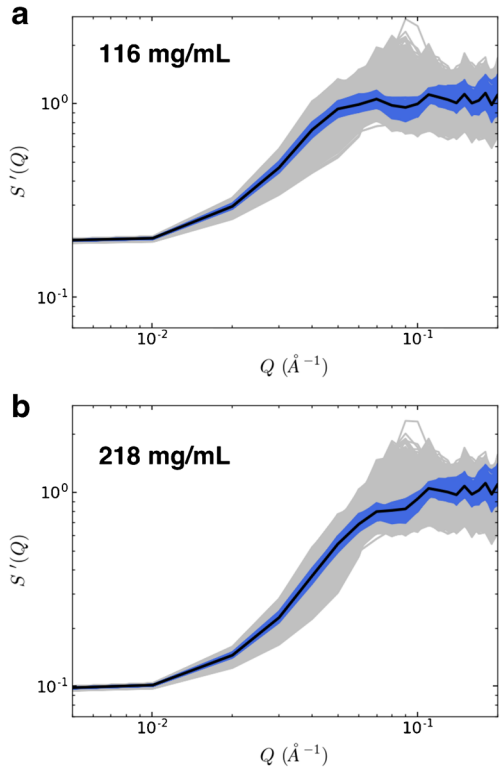

Fig. 5 Effect of configurational fluctuations on the effective structure factor of concentrated NISTmAb solutions with 0 mM NaCl. $S'(Q)$ profiles in gray and blue correspond to NISTmAb ensembles of all and best structures respectively [9]. Black line corresponds to $S'(Q)$ using the experimental data at dilute conditions. **a** 116 mg/mL, **b** 218 mg/mL

from fitting $S'(Q)$ for ensembles of structures. Overall, the parameters were very comparable at all concentrations and statistically equivalent for some conditions. The effective radius varied from ~46 to ~53 Å in most cases and was comparable to the Rg of the NISTmAb (49.0 ± 1.2 Å) [8]. In addition, the effective charge varied from ~ 6 to 16 e in most cases, which agrees with the 11e charge determined experimentally as described below. Consequently, a net repulsive model dominated by electrostatic interactions was appropriate to describe the interactions of NISTmAb in its histidine buffer at a wide range of concentrations. In addition, the resulting parameters were independent of the ensemble selected for the analysis (all structures or best structures). In the case of the effective size, the ensemble with the most fluctuations (all structures) had higher uncertainties, but no changes were observed for the effective charge when comparing the two types of ensembles considered.

Table 1 Parameters for the Hayter and Penfold model describing electrostatic interactions

Concentration in mg/mL – Ensemble	Diameter in Å	Charge in e
28.1 - Best	114 ± 23	18 ± 11
51.9 - Best	98.6 ± 4.3	16 ± 2
116 - Best	92.2 ± 1.6	12 ± 1
157 - Best	91.9 ± 1.4	9.3 ± 1.0
218 - Best	95.2 ± 1.7	7.2 ± 2.4
254 - Best	106 ± 3	5.7 ± 3.1
116 - All	94.4 ± 5.6	12 ± 1

The effective diameter and charge were obtained from the fitting, while the other parameters were fixed as follows: temperature 298 K, salt concentration 12.5 mM, dielectric constant of the solvent 78. The volume fraction was estimated as 0.00132c, where c is protein concentration in mg/mL (see Methods for further details). All and best ensembles correspond to all structures obtained from molecular simulations and structures that best match the experimental data respectively. Uncertainty corresponds to the maximum value between the standard deviation of the ensemble and the uncertainty from the fitting

Viscosity and ELS data were collected on the same samples used for the scattering measurements, in order to correlate the scattering results at high concentration with the properties of NISTmAb solutions in different buffers. Figure 6 presents viscosity data of the NISTmAb at the same conditions measured during the scattering experiments. No differences were observed in the viscosity up to concentrations ~ 100 mg/mL. At high concentrations, the viscosities of NISTmAb solutions with NaCl were higher than the viscosities of solutions with 0 mM NaCl. This can be attributed to the differences in PPI as NaCl screens the surface charge of the NISTmAb. Nonetheless, for the two conditions studied, the viscosities did not exceed the 20 mPa s limit until the concentration was above 170 mg/mL.

ELS was used to measure the effective charge Z_{eff}. The resulting net charge was 4.1 ± 0.4 and −.5 ± 0.5 for the NISTmAb in 0 and 150 mM NaCl respectively (uncertainty corresponds to the standard deviation of 15 measurements). The resulting Debye-Hückel-Henry charge Z_{HDD} was 11 ± 1 and −3 ± 4 for the NISTmAb in 0 and 150 mM NaCl respectively (uncertainty corresponds to ±1 the propagated standard error). These results are in agreement with the parameters of the models used to describe the scattering data of the NISTmAb at intermediate and high concentrations.

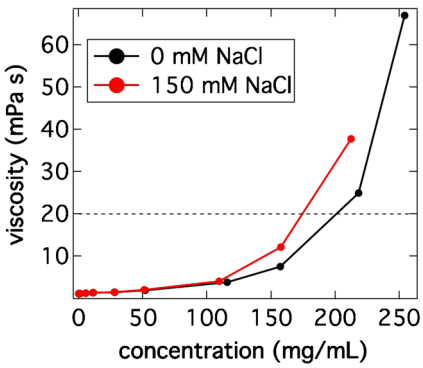

Fig. 6 Viscosity of NISTmAb solutions as a function of concentration. Dashed line at 20 mPa s represents the threshold value at which antibody solutions are generally considered highly viscous [1, 23]. Uncertainties, corresponding to the standard error, are smaller than markers. Lines are used to guide the eye

SANS is not only suitable to study liquid solutions, but it can also be used to measure the scattering of amorphous samples during the freezing and thawing processes (in situ). Figure 7 shows the SANS profiles of frozen and thawed NISTmAb samples in buffer with 0 and 150 mM NaCl. The scattering profiles at 25 °C were in agreement with those of Fig. 2, in which the samples with NaCl had a higher low-Q intensity. No changes in the scattering profiles were observed when decreasing the temperature down to −5 °C. However, a major change in the profile occured after further decreasing the temperature by 5 to −10 °C, the temperature at which the sample was frozen. At this condition, the nearest neighbor peak was clearly observed at ~ 0.2 Å^{-1}, which corresponds to a distance, d, of ~ 32 Å ($d = 2\pi/Q$). Moreover, the low-Q region (length scales larger than ~ 200 Å) displayed a linear upturn in the *logI* vs *logQ* plot, representing protein aggregates and ice cracks as seen in previous studies [14, 15]. When the temperature was further decreased to −80 °C, the peak became more pronounced but did not change its Q position (molecular spacing). The low-Q features did not change at these low temperatures. After thawing the protein sample by increasing the temperature up to 25 °C, the solution features of the scattering profile were fully recovered for both samples in 0 and 150 mM NaCl. The freezing/thawing cycles were repeated three times with no changes in the scattering profiles. In addition, the 2D scattering profiles were isotropic and independent of the cooling and warming rates (data not shown, see Methods for details).

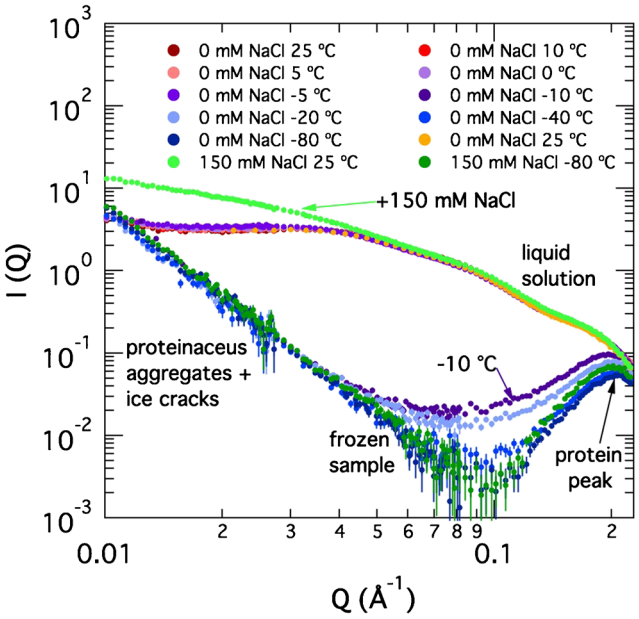

Fig. 7 SANS profile of NISTmAb solutions during freezing and thawing cycles. Protein concentration is 121 and 141 mg/mL for the 0 and 150 mM NaCl samples respectively. Error bars correspond to ±1 the standard error

Discussion

Small-angle scattering is a powerful tool to investigate the distribution of atoms in the molecule and thus molecular correlations in solution or amorphous phases. Measurements can be performed without diluting concentrated samples or changing the conditions of the formulation buffer, making it a suitable technique to study different formulations at various concentrations. Scattering techniques can probe long-range interactions of antibodies in the low-Q region (~ $Q \leq 0.05$ Å^{-1}) of the scattering curve. Small angle X-ray and neutron scattering have a larger angular dependence, that covers the length scales of the internal structure of proteins, compared to static light scattering (SLS) that allows the comparison of scattering profiles from theoretical or computational models with experimental data.

Our small-angle scattering study found that the screening of surface charges played an important role on the net interactions of the NISTmAb in histidine buffer with 0 and 150 mM NaCl. The ELS measurements confirmed the lower Z_{HDD} charge after adding NaCl. In the presence of NaCl, sodium and chlorine ions interacted with the charges on the surface of the protein, leading to charge screening and a decrease in the strength of the repulsive interactions. This analysis is consistent with the $S'(Q)$ results of Figs. 2 and 3. Protein-protein interactions involve a complex interplay of attractive and repulsive non-bonded interactions, resulting from electrostatics, Van der Waals, hydrophobic, hydration, excipient interactions, among others. Note that a net repulsive interaction does not mean that there are no attractive interactions in the system, but only that the net interactions are dominated by repulsion between protein molecules.

In the low-Q region of the small-angle scattering profile, the quantity $S'(0)$ can be calculated at each concentration as shown in Fig. 3d. $S'(0)$ is proportional to the Kirkwood-Buff integral G_{22}, which can be obtained from light scattering experiments [3, 4]. As the concentration of protein approaches zero, $G_{22} \sim -2B_{22}$, where the second virial coefficient B_{22} is commonly used to estimate and compare intermolecular interactions across protein formulations. Because B_{22} can only be calculated from dilute protein solutions, B_{22} was not calculated from the SANS data. However, the conclusions from SANS are consistent with the B_{22} values from static light scattering [18]. Assuming a diameter of 90 Å, $B_{22}^{HS} = 2\pi\sigma^3/2$ for a hard-sphere is 4.2 mol mL/g^2. For the NISTmAb in 0 mM NaCl, $B_{22} > B_{22}^{HS}$ and thus additional repulsive interactions, besides the steric repulsion, are contributing to the net interactions in the system. On the other hand, $0 < B_{22} < B_{22}^{HS}$ for the NISTmAb with 150 mM NaCl, indicating that an attractive component, along with the steric repulsion, yield a net repulsive interaction. Nevertheless, contrary to B_{22}, $S'(0)$ contains information on the interactions of the NISTmAb at high concentrations. Small-angle scattering experiments showed

that this trend in interactions extends to high concentrations of NISTmAb in solution. However, the attractive contribution became weaker in solutions with 150 mM NaCl as the concentration of NISTmAb increases.

The analysis of configurational fluctuations in the $S'(Q)$ profiles shows that the colloidal models used to describe the experimental data were appropriate, regardless of the particular NISTmAb configuration. Moreover, the effective charge and size obtained from the colloidal model fitting at various concentrations were in close agreement with the experimentally obtained charge and radius of gyration. This result suggests that a colloidal model with electrostatic repulsions is a good representation of the NISTmAb in its formulation buffer with 0 mM NaCl at intermediate and high concentrations (up to ~ 254 mg/mL). The ensembles of NISTmAb structures yielded a consistent $S'(Q)$ analysis within the statistical uncertainty, regardless of the ensembles used to carry out the analysis.

Viscosity is a macroscopic property that affects syringeability and injectability of therapeutic protein solutions. Protein-protein interactions, which can be measured with scattering, are one of the most important factors that affect the viscosity of these solutions. Analysis of the SANS data confirmed that intermolecular interactions are affected by formulation and solvent conditions and these interactions have an impact on viscosity. For the conditions studied, higher viscosities were observed after adding NaCl to the formulation buffer. Consequently, an interplay of repulsive and attractive interactions led to an increase in solution viscosity. In the case of the NISTmAb, weakening the repulsive interactions resulted in higher viscosities. However, this was not the case for other antibodies. Previous work [37] reported a decrease in the viscosity of a 150 mg/mL antibody solution after adding a similar concentration of NaCl for one antibody, but no changes in viscosities for another antibody. Clearly intermolecular interactions do affect viscosity, but the effects of salts on the viscosity cannot be generalized from these two cases and understanding their effects requires a detailed knowledge of the intermolecular interactions and other factors that impact the viscosity [29].

The SEC data shows that the NISTmAb was stable at concentrations up to ~ 250 mg/mL after two weeks of storage at 4 °C. Although dilution occured during the SEC measurements, any irreversible aggregation resulting from a crowded environment or the presence of 150 mM NaCl in the buffer would have been detected with SEC.

Finally, SANS is a technique that uniquely allows the study of the freezing process of protein solutions in situ. The scattering profiles in Fig. 7 indicate that the overall structure of the NISTmAb remained unaffected when performing up to three freezing and thawing cycles. However, ice cracks and new solid-air interfaces formed during freezing could promote protein adsorption at interfaces. Upon adsorption, partial changes in secondary structure are likely to occur [33], which can further nucleate aggregation in the bulk solution. These partial changes in secondary structure cannot be easily assessed by SANS. In addition, changes in the scattering intensity showed that the NISTmAb solution froze between −5 and −10 °C under the conditions studied. Note that the freezing point of D^2O is 3.8 °C and thus protein and cosolutes decreased the freezing point. As previously reported for antibodies [10], the presence of a nearest neighbor peak at length scales of ~ 32 Å indicates that antibodies interdigitate in crowded environments to distances of ~ $2Rg/3$ as a result of their flexibility and non-globular structure. Note that phase separation occurs in frozen samples; thus, protein concentrations as high as ~ 600 mg/mL can be obtained in the protein-rich phase [10, 15].

Contrary to previous studies on lysozyme solutions [14, 15], the 2D profiles of the NISTmAb frozen samples were isotropic and independent of the cooling rate. While further research is needed, it is possible that cosolute excipients avoid the formation of structures in the system larger than those probed by SANS (micronsize or larger) and minimize anisotropic features in the stress field of the sample during freezing. Because the scattering profile was fully recovered after freezing and thawing, aggregates formed during these processes were reversible even in the presence of NaCl, which was the case of lysozyme for NaCl concentrations ≤150 mM [14, 15]. Because no differences in the position of the nearest neighbor peak were observed between the 0 and 150 mM NaCl samples, NaCl did not affect the packing structure in the crowded state. This finding is identical to that observed for lysozyme solutions in similar concentrations of NaCl [14, 15], and consistent with the $S'(0)$ trend in Fig. 3d, in which the difference in PPI between the protein solutions with 0 and 150 mM NaCl became less pronounced as protein concentration increased.

Conclusions

Small-angle scattering is not only suitable for studying the conformation and solution structure of the NISTmAb [8], but it can also be used to investigate protein-protein interactions at high concentrations. SANS was used to study intermolecular interactions of the NISTmAb with 0 and 150 mM NaCl. Adding NaCl to the formulation buffer led to adsorption of ions to the surface of the protein and the screening of charges that contribute to a net repulsive interaction between the molecules. Analysis of the effective structure factors from the scattering data indicated that in samples with 0 mM NaCl, the system has a net repulsive interaction as a result of both a steric and an electrostatic repulsion. These results were not affected by configurational fluctuations in solution due to the flexible structure of the NISTmAb, and the same electrostatic model and range of parameters were used to describe the system at various intermediate and high concentrations. For

the samples with 150 mM NaCl, the net interaction in the system was also repulsive, but consisted in a combination of the steric repulsion and an apparent attractive interaction. This result is possibly due to the flexible and non-spherical shape of antibodies, allowing them to approach distances smaller than the hard-core diameter. Because the surface charges on the protein were mostly screened in the presence of NaCl, the electrostatic repulsion between molecules made a negligible contribution to the net interaction.

This result was also confirmed by the small charge measured with ELS for the solution with 150 mM NaCl. $S'(0)$, determined from small-angle scattering experiments, was used to evaluate PPI at high concentrations. Although PPI obtained from B_{22} at low concentrations are qualitatively consistent with the PPI at high concentrations, the difference in PPI for the protein solutions with 0 and 150 mM NaCl decreased as protein concentration increases. Viscosity measurements showed that decreasing the strength of the electrostatic repulsion by adding NaCl led to an increase in the solution viscosity of the NISTmAb.

Moreover, SANS experiments performed during the freezing and thawing cycles in situ showed that the overall structure of the molecule was reversible after up to three cycles. Although a highly crowded environment was observed in the frozen state and some aggregates formed during the freezing process, these species were not detected in the thawed samples. In summary, SANS experiments combined with other biophysical techniques have provided further insights into the colloidal stability of the NISTmAb reference material.

Acknowledgements The authors acknowledge the following scientists for their help and support to this work: Zhiyuan Wang (Tsinghua University) and Yun Liu (NIST, University of Delaware) for their help with SANS data collection, John Schiel (NIST, IBBR) for making the material available for this study and guiding the SEC measurements, Marco Blanco (NIST, IBBR) for discussions on G_{22}, Samiul Amin (previously affiliated with Malvern Instruments) and Neil Lewis (Malvern Instruments) for starting and supporting a collaboration between Malvern and NIST. MMC acknowledges financial support from the NIST biomanufacturing initiative. This work used CCP-SAS software developed through a joint EPSRC (EP/K039121/1) and NSF (CHE-1265821) grant.

Compliance with Ethical Standards

Conflict of interest All authors of this article declare no conflict of interest.

References

1. Agrawal NJ, Helk B, Kumar S, Mody N, Sathish HA, Samra HS, et al. Computational tool for the early screening of monoclonal antibodies for their viscosities. MAbs. 2016;8(1):43–8.
2. Apfel U, Grunder R, Ballauff M. A turbidity study of particle interaction in latex suspensions. Colloid Polym Sci. 1994;272(7):820–9.
3. Blanco MA, Sahin E, Li Y, Roberts CJ. Reexamining protein-protein and protein-solvent interactions from kirkwood-buff analysis of light scattering in multicomponent solutions. J Chem Phys. 2011;134(22):225–103.
4. Blanco MA, Perevozchikova T, Martorana V, Manno M, Roberts CJ. Protein-protein interactions in dilute to concentrated solutions: *a*-chymotrypsinogen in acidic conditions. J Phys Chem B. 2014;118(22):5817–31.
5. Brookes EH, Anjum N, Curtis JE, Marru S, Singh R, Pierce M. Genapp module execution and airavata integration. In: 2014 9th gateway computing environments workshop, pp. 9–12 2014.
6. Carpenter JF, Randolph TW, Jiskoot W, Crommelin DJA, Middaugh CR, Winter G, et al. Overlooking subvisible particles in therapeutic protein products: gaps that may compromise product quality. J Pharm Sci. 2009;98(4):1201–5.
7. Carrasco B, de la Torre JG, Davis KG, Jones S, Athwal D, Walters C, et al. Crystallohydrodynamics for solving the hydration problem for multi-domain proteins: open physiological conformations for human igg. Biophys Chem. 2001;93(2–3):181–96.
8. Castellanos MM, Mattison K, Krueger S, Curtis JE. Characterization of the NISTmAb Reference Material using small-angle scattering and molecular simulation. Part I: Dilute solution structures. Anal Bioanal Chem. 2018. https://doi.org/10.1007/s00216-018-0868-2.
9. Castellanos MM, Pathak JA, Leach W, Bishop SM, Colby RH. Explaining the non-newtonian character of aggregating monoclonal antibody solutions using small-angle neutron scattering. Biophys J. 2014;107(2):469–76.
10. Castellanos MM, Clark NJ, Watson MC, Krueger S, McAuley A, Curtis JE. Role of molecular flexibility and colloidal descriptions of proteins in crowded environments from small-angle scattering. J Phys Chem B. 2016;120(49):12,511–8.
11. Castellanos MM, McAuley A, Curtis JE. Investigating structure and dynamics of proteins in amorphous phases using neutron scattering. Comput Struct Biotechnol J. 2016;15:117–30.
12. Chen SH, Bendedouch D. Structure and interactions of proteins in solution studied by small-angle neutron scattering. In: Enzyme structure part K. Methods in enzymology vol 130, pp. 79–116. Academic Press 1986. https://doi.org/10.1016/0076-6879(86)30009-0
13. Chen SH, Broccio M, Liu Y, Fratini E, Baglioni P. The two-yukawa model and its applications: the cases of charged proteins and copolymer micellar solutions. J Appl Crystallogr. 2007;40:S321–6.
14. Curtis JE, McAuley A, Nanda H, Krueger S. Protein structure and interactions in the solid state studied by small-angle neutron scattering. Faraday Discuss. 2012;158:285–99.
15. Curtis JE, Nanda H, Khodadadi S, Cicerone M, Lee HJ, McAuley A, et al. Small-angle neutron scattering study of protein crowding in liquid and solid phases: lysozyme in aqueous solution, frozen solution, and carbohydrate powders. J Phys Chem B. 2012;116(32):9653–67.
16. Curtis JE, Raghunandan S, Nanda H, Krueger S. Sassie: a program to study intrinsically disordered biological molecules and macromolecular ensembles using experimental scattering restraints. Comput Phys Commun. 2012;183(2):382–9.
17. Godfrin PD, Zarraga IE, Zarzar J, Porcar L, Falus P, Wagner NJ, et al. Effect of hierarchical cluster formation on the viscosity of concentrated monoclonal antibody formulations studied by neutron scattering. J Phys Chem B. 2016;120(2):278–91.
18. Gokarn Y, Agarwal S, Arthur K, Bepperling A, Day ES, Filoti D, et al. Biophysical techniques for characterizing the higher order structure and interactions of monoclonal antibodies, chap. 6, pp. 285–327. ACS Symposium Series. 2015.
19. Hammouda B. Probing nanoscale structures-the sans toolbox. Gaithersburg: Natl. Institute Standards Technology Center for Neutron Research 2016. https://www.ncnr.nist.gov/staff/hammouda/the_SANS_toolbox.pdf.

20. Hayter JB, Penfold J. An analytic structure factor for macroion solutions. Mol Phys. 1981;42(1):109–18.
21. Inouye H, Houde D, Temel DB, Makowski L. Utility of solution x-ray scattering for the development of antibody biopharmaceuticals. J Pharm Sci. 2016;105(11):3278–89.
22. Kline S. Reduction and analysis of sans and usans data using igor pro. J Appl Crystallogr. 2006;39(6):895–900.
23. Li L, Kumar S, Buck P, Burns C, Lavoie J, Singh S, et al. Concentration dependent viscosity of monoclonal antibody solutions: explaining experimental behavior in terms of molecular properties. Pharm Res. 2014;31(11):3161–78.
24. Liu Y, Chen WR, Chen SH. Cluster formation in two-yukawa fluids. J Chem Phys. 2005;122(4):044,507–13.
25. Mosbæk CR, Konarev PV, Svergun DI, Rischel C, Vestergaard B. High concentration formulation studies of an igg2 antibody using small angle x-ray scattering. Pharm Res. 2012;29(8):2225–35.
26. Perkins SJ, Wright DW, Zhang H, Brookes EH, Chen J, Irving TC, et al. Atomistic modelling of scattering data in the Collaborative Computational Project for Small Angle Scattering (CCP-SAS). J Appl Crystallogr. 2016;49(6):1861–75.
27. Roberts CJ. Therapeutic protein aggregation: mechanisms, design, and control. Trends Biotechnol. 2014;32(7):372–80.
28. Roberts CJ, Wang W. Aggregation of therapeutic proteins. 1edn ed. New York: Wiley; 2010.
29. Sarangapani PS, Weaver J, Parupudi A, Besong TMD, Adams GG, Harding SE, et al. Both reversible self-association and structural changes underpin molecular viscoelasticity of mab solutions. J Pharm Sci. 2016;105(12):3496–506.
30. Schiel JE, Davis DL, Borisov OV. State-of-the-art and emerging technologies for therapeutic monoclonal antibody characterization volume 1. monoclonal antibody therapeutics: Structure, function, and regulatory space. In: Schiel JE, Davis DL, Borisov OV, editors. State-of-the-art and emerging technologies for therapeutic monoclonal antibody characterization volume 1. Monoclonal antibody therapeutics: structure, function, and regulatory space, vol 1, pp. ix–xi. ACS Symposium Series. 2014.
31. Schiel JE, Davis DL, Borisov OV. State-of-the-art and emerging technologies for therapeutic monoclonal antibody characterization volume 2. biopharmaceutical characterization: the nistmab case study. In: Schiel JE, Davis DL, Borisov OV, editors. State-of-the-art and emerging technologies for therapeutic monoclonal antibody characterization volume 2. Biopharmaceutical characterization: the NISTmAb case study, pp. ix–xii. ACS Symposium Series. 2015.
32. Schiel JE, Davis DL, Borisov OV. State-of-the-art and emerging technologies for therapeutic monoclonal antibody characterization volume 3. defining the next generation of analytical and biophysical techniques. In: Schiel JE, Davis DL, Borisov OV, editors. State-of-the-art and emerging technologies for therapeutic monoclonal antibody characterization volume 3. Defining the next generation of analytical and biophysical techniques, pp. ix–x. ACS Symposium Series. 2015.
33. Schwegman JJ, Carpenter JF, Nail SL. Evidence of partial unfolding of proteins at the ice/freeze-concentrate interface by infrared microscopy. J Pharm Sci. 2009;98(9):3239–46.
34. Shire SJ, Shahrokh Z, Liu J. Challenges in the development of high protein concentration formulations. J Pharm Sci. 2004;93(6):1390–402.
35. Velev OD, Kaler EW, Lenhoff AM. Protein interactions in solution characterized by light and neutron scattering: comparison of lysozyme and chymotrypsinogen. Biophys J. 1998;75(6):2682–97.
36. Yearley EJ, Zarraga IE, Shire SJ, Scherer TM, Gokarn Y, Wagner NJ, et al. Small-angle neutron scattering characterization of monoclonal antibody conformations and interactions at high concentrations. Biophys J. 2013;105(3):720–31.
37. Yearley EJ, Godfrin PD, Perevozchikova T, Zhang H, Falus P, Porcar L, et al. Observation of small cluster formation in concentrated monoclonal antibody solutions and its implications to solution viscosity. Biophys J. 2014;106(8):1763–70.